

## MODELING OF DEBRIS DISKS IN SINGLE AND BINARY STARS

L. García and M. Gómez

Observatorio Astronómico de Córdoba (OAC), Argentina

Received April 20 2015; accepted July 8 2016

### RESUMEN

Los telescopios espaciales *Spitzer* y *Herschel* han permitido incrementar el número de posibles análogos del Cinturón de Kuiper en otras estrellas, tanto en sistemas individuales como en binarios. El objetivo de este trabajo es caracterizar los discos de escombros en estos 2 tipos de estrellas e identificar propiedades comunes, así como, posibles diferencias. Para ello, se recopilaron 2 muestras de 25 estrellas individuales y 14 sistemas binarios (edades  $> 100 \times 10^6$  años) con flujos observados para  $\lambda > 100 \mu\text{m}$  y evidencia de excesos en emisión en el infrarrojo atribuidos a la presencia de disco. Luego, se construyeron y modelaron las distribuciones especiales de energía (SEDs), y se compararon los parámetros obtenidos para los discos de ambas muestras. En general, los discos tienen una región interna ( $< 3\text{-}5$  UA), relativamente libre de polvo y se extenderían más allá de 100 UA. No se encontraron diferencias significativas en las distribuciones de masa y de tamaño de las partículas de polvo de ambas muestras.

### ABSTRACT

Infrared space observatories such as *Spitzer* and *Herschel* have allowed the detection of likely analogs to the Kuiper Belt in single as well as binary systems. The aim of this work is to characterize debris disks in single and binary stars and to identify features shared by the disks in both types of systems, as well as possible differences. We compiled a sample of 25 single and 14 binary stars (ages  $> 100$  Myr) with flux measurements at  $\lambda > 100 \mu\text{m}$  and evidence of infrared excesses attributed to the presence of debris disks. Then, we constructed and modeled the observed spectral energy distributions (SEDs), and compared the parameters of the disks of both samples. Both types of disks are relatively free of dust in the inner region ( $< 3\text{-}5$  AU) and extend beyond 100 AU. No significant differences in the mass and dust size distributions of both samples are found.

*Key Words:* binaries: general — Kuiper belt: general — protoplanetary disks — stars: solar-type — zodiacal dust

### 1. INTRODUCTION

In the 1980's, the Infrared Astronomical Satellite (*IRAS*) detected emission excesses with respect to the stellar photosphere in well-known nearby main-sequence stars (Aumann et al. 1984; Backman & Paresce 1993). These infrared excesses were associated with dust grains in circumstellar disks. However, the dust cannot be only decaying remnants of the primordial disk. The radiation pressure and the Poynting-Robertson drag (P-R drag), remove dust grains on time-scales several orders of magnitude shorter than the age of the systems (Krivov 2010). For example, in the Solar System, P-R drag removes

dust grains with sizes of  $\approx 10 \mu\text{m}$  in about  $10^5$  yr (Fixsen & Dwek 2002). The disks must be replenished of dust by some kind of mechanism.

Taking the Solar System as reference, it was proposed that the collisions between bodies such as those constituting the Asteroid and Kuiper Belts are the main source of the dust in the disks (Harper et al. 1984; Weissman 1984; Zuckerman & Becklin 1993). Since they would be populated by such bodies, these type of disks are known as "debris disks". An important issue is the origin of the bodies: these objects would be the leftovers or "debris" of a planetary formation process. Collisions can be

triggered by embedded planets capable of perturbing the smaller planetesimals, inducing a collisional cascade that slowly grinds them to dust (Kenyon & Bromley 2001, 2004). Kenyon & Bromley (2002) have also shown that interactions with a star passing by are another mechanism capable of triggering collisional cascades that release dust into the disks.

The first debris disks discovered with *IRAS* were mainly associated with *A*- and *F*-type stars. Subsequently, this type of disks was also detected in later spectral type stars and particularly around *G*-type stars (Decin et al. 2000; Habing et al. 2001). Nevertheless, these disks were confined to the brightest and closest targets (Bryden et al. 2006). Instruments such as MIPS (Multiband Imaging Photometer for Spitzer, Rieke et al. 2004) on board of the *Spitzer* space telescope made feasible a more detailed analysis of the frequency of these structures around Sun-like stars (see, for example, Trilling et al. 2008). More recent observations with the *Herschel* infrared telescope (Pilbratt et al. 2010) have revealed that about 20% of solar-type stars have evidence of debris disks (Eiroa et al. 2013). These observations have also provided a higher fraction of thermally resolved disks than previous missions (Booth et al. 2013; Pawellek et al. 2014).

The study of debris disks is of great interest because it can provide clues to the formation and later evolution of extrasolar planetary systems, as well as the Solar System. In addition, debris disks have been detected not only around single stars, but also around main-sequence binary systems (Trilling et al. 2007). Recent studies have reported that  $\approx$ 10-20% of binary stars have debris disks (Rodriguez & Zuckerman 2012; Eiroa et al. 2013; Rodriguez et al. 2015). However, there may be a dependence of the disk frequency on the spectral type (Thureau et al. 2014; Rodriguez et al. 2015). Debris disks in binary systems are relevant for several reasons: (1) About 45% of Sun-like stars are binaries or higher-order multiple star systems (Duquennoy & Mayor 1991; Raghavan et al. 2010; Duchêne & Kraus 2013; Tokovinin 2014), (2) Most of the stars with known extrasolar planets have *G* spectral types (The Extrasolar Planets Encyclopaedia<sup>1</sup>, The Exoplanet Data Explorer<sup>2</sup>), (3) A significant fraction of planet-host stars ( $\approx$  25%) are, actually, binaries or multiple systems (Raghavan et al. 2006; Desidera & Barbieri 2007) although this percentage is probably a lower limit.

In this contribution, we model the observed spectral energy distributions (SEDs) of 25 single and 14

binary stars with ages  $>$  100 Myr. The objects in both samples have flux measurements at  $\lambda > 100 \mu\text{m}$  and emission excesses at infrared wavelengths attributed to circumstellar disks. The aim of this work is to characterize debris disks previously detected in binary systems and to compare their parameters with those of debris disks around single stars. In § 2 we present the samples, briefly describe the code used and the procedure adopted for the SED modeling. Results are discussed in § 3. Finally, in § 4, we present our conclusions.

## 2. SED MODELING

### 2.1. *The samples*

We compiled a sample of 25 single stars and 14 binary systems selected from published data of *Spitzer* campaigns (such as in: Beichman et al. 2005b, 2006; Bryden et al. 2006; Trilling et al. 2007, 2008; Hillenbrand et al. 2008), some of which were also observed by *Herschel* afterwards. All these stars have IR excesses likely to be produced by debris disks. We restricted the ages to  $>$  100 Myr to avoid including protoplanetary disks, or disks in a transitional phase (see, for example, Espaillat et al. 2012). The objects in both samples have flux measurements at  $\lambda > 100 \mu\text{m}$  available in the literature. Infrared and submillimeter observations are essential to reveal the presence of cold and large dust grains, not detected at shorter wavelengths. In this sense, measurements at  $\lambda > 100 \mu\text{m}$  have an impact on the estimated mass of dust, and on the modeling of the SEDs in general. The availability of submillimeter fluxes is rather limited and restricts the number of systems that can be included in our samples. This is particularly critical for main sequence binary stars. Although the number of objects that meet these selection criteria is rather small, it is interesting to conduct an initial comparison between single and binary stars to search for differences in the characteristics of the debris disks in these two groups.

Binary systems were selected with separations large enough to ensure that the debris disks are around the primary components and to avoid contamination of the photometry by the companion star (particularly at the longest wavelengths). Basic properties of the objects in the single and binary samples are listed in Tables 1 and 2. For the binary stars, the parameters correspond to the primary component. Table 2 also provides the projected separation between the components ( $A_{\text{bin}}$ ). The binary stars HD 13161 and HD 35850 with small angular separations ( $<0.01$  and  $0.0008''$ , respectively) are

<sup>1</sup><http://exoplanet.eu/>

<sup>2</sup><http://exoplanets.org/>

TABLE 1  
SINGLE STARS PROPERTIES

| HD<br>(number) | <i>d</i><br>(pc) | <i>V</i> | Spectral<br>Type | <i>L</i><br>( $L_{\odot}$ ) | Age <sup>a</sup><br>(Gyr) |
|----------------|------------------|----------|------------------|-----------------------------|---------------------------|
| 377            | 38.8             | 7.6      | G2 V             | 1.2                         | 4.1                       |
| 8907           | 34.2             | 6.7      | F8 V             | 2.0                         | 4.2                       |
| 10647          | 17.3             | 5.5      | F9 V             | 1.5                         | 1.9                       |
| 17925          | 10.4             | 6.0      | K1 V             | 0.4                         | 6.2                       |
| 23484          | 16.0             | 7.8      | K3 V             | 0.4                         | 0.6                       |
| 27290          | 20.5             | 4.2      | F1 V             | 6.5                         | 0.3                       |
| 30495          | 13.3             | 5.5      | G2 V             | 0.9                         | 1.2                       |
| 61005          | 35.3             | 8.2      | G9 V             | 0.5                         | 4.1                       |
| 90089          | 21.5             | 5.3      | F4 V             | 2.7                         | 0.3                       |
| 92945          | 21.4             | 7.7      | K1 V             | 0.4                         | 6.5                       |
| 104860         | 47.9             | 7.9      | F8 V             | 1.5                         | 5.3                       |
| 107146         | 28.5             | 7.1      | G2 V             | 1.0                         | 2.4                       |
| 109085         | 18.2             | 4.3      | F2 V             | 5.6                         | 1.6                       |
| 110897         | 17.4             | 6.0      | G0 V             | 1.0                         | 6.5                       |
| 115617         | 8.5              | 4.7      | G7 V             | 0.9                         | 5.3                       |
| 128167         | 15.5             | 4.5      | F2 V             | 3.4                         | 1.4                       |
| 139664         | 17.5             | 4.6      | F4 V             | 3.5                         | 1.2                       |
| 145229         | 33.0             | 7.4      | G0 V             | 1.0                         | 1.3                       |
| 170773         | 37.0             | 6.2      | F5 V             | 3.6                         | 1.7                       |
| 172167         | 7.8              | 0.03     | A0 V             | 53.0                        | 0.2                       |
| 191089         | 53.5             | 7.2      | F5 V             | 3.1                         | 2.6                       |
| 195627         | 27.8             | 4.7      | F0 V             | 7.8                         | 0.2                       |
| 199260         | 21.0             | 5.7      | F6 V             | 1.7                         | 2.3                       |
| 201219         | 35.9             | 8.0      | G5 V             | 0.7                         | 6.7                       |
| 212695         | 46.5             | 6.9      | F5 V             | 2.8                         | 1.4                       |

<sup>a</sup>Ages are from Holmberg et al. (2009) and Casagrande et al. (2011) except for HD 172167 (Song et al. 2000).

probably associated with circumbinary disks, and they will be treated as single stars in our analysis. The median distances for single and binary systems are 21.4 and 19.1 pc, respectively. Median luminosities are  $\approx 1.5 L_{\odot}$ , for single, and  $\approx 1.8 L_{\odot}$ , for binary stars. The stars in the samples are predominantly late-*F* and early-*G* type stars.

To construct the observed SEDs we collected data from several catalogs (such as *Hipparcos*, *2MASS*, *WISE*, etc.) using the tool “Photometry Viewer”<sup>3</sup> from the Vizier Catalogue service. These data were complemented with observations from *Herschel*, *Spitzer*, and surveys at submillimeter wavelengths published in the literature. The fluxes (at  $\lambda > 22 \mu\text{m}$ ) used to construct the observed SEDs are listed in Appendix A.

## 2.2. Modeling procedure

The SEDs were modeled with the code of Wolf & Hillenbrand (2003)<sup>4</sup>. This code calculates the stellar radiation that is scattered and re-emitted by dust

grains that are assumed to be spherical with a homogeneous chemical composition. Then, the capability of the dust grains to scatter, absorb, and re-emit the stellar radiation is described by the scatter and absorption efficiencies ( $Q_{\text{sca}}(\lambda)$ ,  $Q_{\text{abs}}(\lambda)$ ), providing a better description of the dust emission than the blackbody model approach. The stellar continuum is represented by the emission of a blackbody. We fixed the effective temperature ( $T_{\text{eff}}$ ), and the stellar luminosity ( $L$ ) according to the spectral type of the star. The corresponding  $T_{\text{eff}}$  was derived from the calibration of Kenyon & Hartmann (1995). A blackbody for the stellar continuum is a simple but adequate model for the SED modeling proposed, since the fluxes in broad-band filters are fitted.

The disk parameters are: the inner ( $a_{\text{in}}$ ) and outer ( $a_{\text{out}}$ ) radii, the mass ( $M_{\text{dust}}$ ), the radial distribution ( $N(a)$ ) and the size distribution ( $N(D)$ ) of the dust grains, the minimum ( $D_{\text{min}}$ ) and maximum ( $D_{\text{max}}$ ) sizes of the grains, and the chemical composition.

The radial distribution is described by a power-law of the form:

$$N(a) = a^{-q}, \quad (1)$$

where  $N(a)$  is the density of dust grains at the radial distance  $a$  from the central source. The code allows to vary the index  $q$ . Several mechanisms affect the distribution of dust grains in the disks, for example: the P-R drag, the radiation pressure, the collisions between bodies, the presence of massive objects embedded in the disk, etc.

Disk images suggest that the radial distribution of dust is not given by a single law of the form of equation (1) (see, for example, Kalas et al. 2005; Schneider et al. 2005). Indeed, when a power-law can be fitted, the observations show that the  $q$  index varies from  $q = 1$  to  $q = 3$  (Metchev et al. 2005; Kalas et al. 2006; Schneider et al. 2006; Fitzgerald et al. 2007; Maness et al. 2008). In addition, there are a few examples outside this range (Augereau et al. 1999; Kalas et al. 2006).

In pre-main sequence T-Tauri stars (ages of  $\approx 10^6$  yr),  $q$  lies between 1.9 and 2.4 (see, e.g., Kenyon & Hartmann 1987; D’ Alessio et al. 1999; Chiang & Goldreich 1999) and it is expected that  $q$  in debris disks will lie in the same range (Wolf & Hillenbrand 2003). In addition, for the Solar System,  $q$  varies from  $q = 1.0$  to  $q = 2.4$  (Gor’kavyi et al. 1997; Kelsall et al. 1998), depending on the distance to the Sun. In this work, we adopted  $q = 1.5$  in an attempt to select a value as representative as possible for most of the analyzed systems.

<sup>3</sup>The website of Photometry Viewer: <http://vizier.u-strasbg.fr/vizier/sed/>

<sup>4</sup>In this work, we used the version available at <http://www1.astrophysik.uni-kiel.de/dds/>

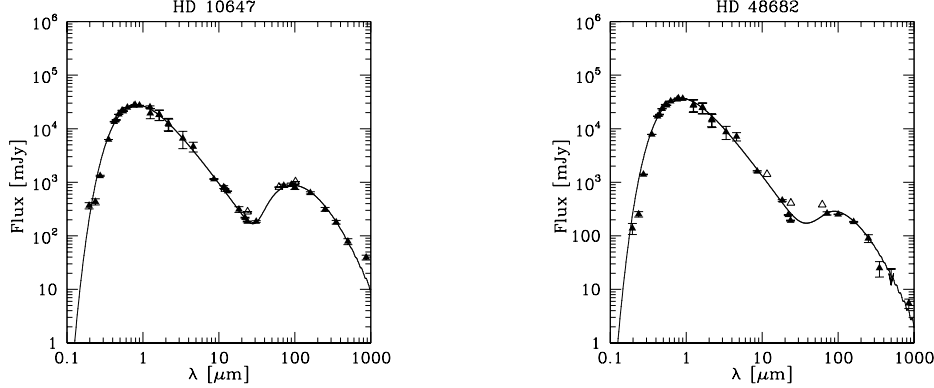


Fig. 1. Left panel: SED model for a single star (HD 10647). Right panel: SED model for a binary system (HD 48682). Triangles indicate actual fluxes and arrows upper limits. Error bars for fluxes at different wavelengths are included. Observations from IRAS are indicated with empty triangles but were not used in the modeling. The complete sets of modeled SEDs for single and binary stars, listed in Table 3, are shown in Figure 4 and 5, respectively.

TABLE 2  
BINARY STARS PROPERTIES

| HD<br>(number)     | $d$<br>(pc) | $V$  | Spectral<br>Type | $L$<br>( $L_{\odot}$ ) | $A_{\text{bin}}^{\text{a}}$<br>('') | $A_{\text{bin}}$<br>(AU) | Age <sup>b</sup><br>(Gyr) |
|--------------------|-------------|------|------------------|------------------------|-------------------------------------|--------------------------|---------------------------|
| 1404               | 41.3        | 4.5  | A2 V             | 26.1                   | 6.6                                 | 272                      | 0.5                       |
| 19994              | 22.6        | 5.1  | F8.5 V           | 4.0                    | 6.8                                 | 154                      | 5.7                       |
| 20807              | 12.0        | 5.2  | G0 V             | 1.0                    | 309.1                               | 3708                     | 7.8                       |
| 38393              | 8.9         | 4.1  | F6 V             | 2.5                    | 95.8                                | 853                      | 1.3                       |
| 48682              | 16.5        | 5.2  | G0 V             | 1.8                    | 36.2                                | 598                      | 1.3                       |
| 91312              | 34.6        | 4.7  | A7 IV            | 12.0                   | 16.9                                | 585                      | 0.2                       |
| 102647             | 10.9        | 2.1  | A3 V             | 14.0                   | 39.7                                | 433                      | 0.3                       |
| 139323             | 22.4        | 7.5  | K3 V             | 0.4                    | 121.8                               | 2728                     | 5.0                       |
| 139813             | 21.7        | 7.3  | G5 V             | 0.6                    | 31.7                                | 688                      | 9.5                       |
| 161897             | 28.9        | 7.6  | K0 V             | 0.6                    | 90.0                                | 2601                     | 2.0                       |
| 207129             | 15.6        | 5.5  | G2 V             | 1.3                    | 55.0                                | 858                      | 5.2                       |
| 216956             | 7.7         | 1.2  | A4 V             | 17.0                   | 7062.3                              | 54401                    | 0.4                       |
| 13161 <sup>c</sup> | 38.11       | 3.00 | A5 III           | 78.0                   | <0.01                               | 0.4                      | 0.7                       |
| 35850 <sup>c</sup> | 36.84       | 6.31 | F8 V             | 1.8                    | 0.0008                              | 0.03                     | 4.3                       |

<sup>a</sup>Separations are from the Catalog of Components of Double & Multiple stars (on-line version at: <http://vizier.u-strasbg.fr/viz-bin/VizieR-3?-source=I/274/ccdm>) except for: HD 13161 (Trilling et al. 2007), HD 38393, HD 102647 (Mason et al. 2001), HD 35850 and HD 216956 (Rodriguez & Zuckerman 2012).

<sup>b</sup>Ages are from Holmberg et al. (2009) and Casagrande et al. (2011) except for: HD 91312, HD 139323 (Rhee et al. 2007), HD 13161 (Vican 2012), HD 102647 (David & Hillenbrand 2015), HD 161897 (Carpenter et al. 2009) and HD 216956 (Mamajek 2012).

<sup>c</sup> Binary separation < 0.01''. Likely circumbinary disk.

The size distribution of the dust grains is also described by a power-law function:

$$N(D) = D^{-x}, \quad (2)$$

$N(D)$  is the number of dust grains with size  $D$ , within the interval  $(D_{\min}, D_{\max})$ . We assumed the same size distribution for all the disks in our sample and set a value of the index  $x = 3.5$ . This corresponds to the size distribution of an infinite collisional cascade (Dohnanyi 1969).

In debris disks, dust particles are generated through collisions of parent bodies. The collisional life-time is much shorter than the P-R drag time for known debris disks. This means that planetesimals are ground up into dust particles, small enough to be removed by the radiation pressure, before the P-R drag produces any appreciable effect. Thus, the P-R drag can be ignored in known debris disks (Dominik & Decin 2003; Wyatt 2005). In this context, the radiation pressure sets a lower limit to the size of the dust grains, and collisions prevail as the dominating

TABLE 3  
MODEL PARAMETERS FOR THE DISKS IN SINGLE AND BINARY STARS

| Single stars   |                         |                          |   |                          |                          |                   | Binary stars       |                         |                          |   |                          |                          |                  |
|----------------|-------------------------|--------------------------|---|--------------------------|--------------------------|-------------------|--------------------|-------------------------|--------------------------|---|--------------------------|--------------------------|------------------|
| HD<br>(number) | $a_{\text{in}}$<br>(AU) | $a_{\text{out}}$<br>(AU) | $M_{\text{dust}}$<br>(M <sub>Moon</sub> ) | $D_{\text{min}}$<br>(μm) | $D_{\text{max}}$<br>(μm) | $(F_{850}/F_*)$   | HD<br>(number)     | $a_{\text{in}}$<br>(AU) | $a_{\text{out}}$<br>(AU) | $M_{\text{dust}}$<br>(M <sub>Moon</sub> ) | $D_{\text{min}}$<br>(μm) | $D_{\text{max}}$<br>(μm) | $(F_{850}/F_*)$  |
| 377            | 10                      | 150                      | 1.35                                      | 10                       | 450                      | 179               | 1404               | 50                      | 250                      | 0.03                                      | 10                       | 400                      | 3 <sup>a</sup>   |
| 8907           | 50                      | 200                      | 1.22                                      | 5                        | 180                      | 102               | 19994              | 50                      | 200                      | 0.05                                      | 20                       | 250                      | 4 <sup>a</sup>   |
| 10647          | 25                      | 160                      | 1.08                                      | 5                        | 500                      | 278               | 20807              | 50                      | 150                      | 0.13                                      | 170                      | 250                      | 33 <sup>a</sup>  |
| 17925          | 21                      | 560                      | 0.51                                      | 4                        | 597                      | 36                | 38393              | 40                      | 90                       | 0.01                                      | 10                       | 180                      | 2                |
| 23484          | 10                      | 150                      | 0.21                                      | 20                       | 380                      | 32 <sup>a</sup>   | 48682              | 10                      | 150                      | 0.16                                      | 10                       | 390                      | 26               |
| 27290          | 65                      | 150                      | 0.11                                      | 6                        | 300                      | 7 <sup>a</sup>    | 91312              | 250                     | 570                      | 1.89                                      | 200                      | 490                      | 43 <sup>a</sup>  |
| 30495          | 12                      | 100                      | 0.03                                      | 8                        | 12 <sup>a</sup>          | 6                 | 102647             | 10                      | 150                      | 0.03                                      | 5                        | 400                      | 5                |
| 61005          | 8                       | 200                      | 4.06                                      | 5                        | 230                      | 538 <sup>a</sup>  | 139323             | 25                      | 100                      | 1.76                                      | 15                       | 160                      | 230 <sup>a</sup> |
| 90089          | 45                      | 350                      | 0.35                                      | 40                       | 350                      | 27 <sup>a</sup>   | 139813             | 80                      | 160                      | 2.14                                      | 50                       | 220                      | 44               |
| 92945          | 11                      | 100                      | 0.76                                      | 9                        | 350                      | 192               | 161897             | 65                      | 155                      | 4.06                                      | 60                       | 290                      | 539              |
| 104860         | 45                      | 290                      | 4.33                                      | 6                        | 200                      | 365               | 207129             | 20                      | 100                      | 0.20                                      | 10                       | 400                      | 25               |
| 107146         | 16                      | 263                      | 4.33                                      | 7                        | 608 <sup>a</sup>         | 481               | 216956             | 25                      | 250                      | 0.54                                      | 15                       | 280                      | 30               |
| 109085         | 3                       | 350                      | 0.49                                      | 30                       | 500                      | 44                | 13161 <sup>b</sup> | 30                      | 350                      | 0.18                                      | 8                        | 80                       | 1 <sup>a</sup>   |
| 110897         | 15                      | 120                      | 0.09                                      | 50                       | 480                      | 22 <sup>a</sup>   | 35850 <sup>b</sup> | 37                      | 211                      | 0.76                                      | 8                        | 140                      | 70               |
| 115617         | 8                       | 190                      | 0.08                                      | 50                       | 200                      | 11                |                    |                         |                          |   |                          |                          |                  |
| 128167         | 3                       | 580                      | 0.35                                      | 73                       | 590                      | 20                |                    |                         |                          |   |                          |                          |                  |
| 139664         | 18                      | 300                      | 1.03                                      | 20                       | 250                      | 63 <sup>a</sup>   |                    |                         |                          |   |                          |                          |                  |
| 145229         | 17                      | 250                      | 0.54                                      | 6                        | 300                      | 60 <sup>a</sup>   |                    |                         |                          |   |                          |                          |                  |
| 170773         | 70                      | 110                      | 2.6                                       | 9                        | 250                      | 278               |                    |                         |                          |   |                          |                          |                  |
| 172167         | 15                      | 239                      | 0.16                                      | 15                       | 299                      | 6                 |                    |                         |                          |   |                          |                          |                  |
| 191089         | 5                       | 380                      | 15.16                                     | 17                       | 600                      | 854 <sup>a</sup>  |                    |                         |                          |   |                          |                          |                  |
| 195627         | 55                      | 200                      | 0.65                                      | 7                        | 270                      | 73                |                    |                         |                          |   |                          |                          |                  |
| 199260         | 30                      | 250                      | 0.02                                      | 1                        | 400                      | 2.9 <sup>a</sup>  |                    |                         |                          |   |                          |                          |                  |
| 201219         | 15                      | 330                      | 5.95                                      | 100                      | 400                      | 1000 <sup>a</sup> |                    |                         |                          |   |                          |                          |                  |
| 212695         | 50                      | 250                      | 1.87                                      | 50                       | 300                      | 164               |                    |                         |                          |   |                          |                          |                  |

<sup>a</sup>For systems with no data at 850 μm, we used values from the SEDs modeling.

<sup>b</sup>Binary separation <0.01''. Likely circumbinary disk.

process that governs the size of the dust grains. Estimations of index  $x$  from observations show values that are in agreement with a collisional cascade, although several cases are outside the expected range (Mittal et al. 2015).

We adopted a chemical composition of 100% astronomical silicates for all the disks in our samples (Draine & Lee 1984; Weingartner & Draine 2001). While observations show that dust grains in debris disks are not composed exclusively of astronomical silicates (for example, HD 69830, Beichman et al. 2005a;  $\beta$  Pictoris, Chen et al. 2007; or even the Solar System, Greenberg 1998; Reach et al. 2003), and that the composition is not the same from one disk to another, it is likely that the main constituent of the dust are the astronomical silicates (Pollack et al. 1994).

The fitted parameters in our modeling were: the inner and outer radii of the disks ( $a_{\text{in}}$ ,  $a_{\text{out}}$ ), the mass of dust ( $M_{\text{dust}}$ ), and the minimum and maximum sizes of the dust grains ( $D_{\text{min}}$ ,  $D_{\text{max}}$ ). For each star, we constructed several models varying these parameters. We chose the one that best reproduced the observed fluxes and minimized the residuals through the chi-squared determination. We adopted fixed

values for  $q$ ,  $x$ , and the chemical composition to reduce the number of fitted parameters. For these parameters, we assumed values provided by current theories of debris disks as explained above.

### 3. RESULTS

The resulting parameters from the SED modeling are listed in Table 3. Figure 1 shows two examples of the modeled SEDs for a single star (HD 10647, left panel) and a binary system (HD 48682, right panel). The complete sets of SEDs models (for both groups, single and binary stars) are presented in Appendix B. In this section, we compare and analyze the characteristics of the debris disks in both samples of stars.

#### 3.1. Inner and Outer Radii

Histograms of the inner radii distributions for our samples are shown in the left panel of Figure 2. The median values of the inner radii for debris disks in single and binary stars are 17 and 38 AU, respectively. The statistical Kolmogorov-Smirnov test (K-S test, Press et al. 1992) indicated a probability of 0.1 (p-value) that both radii distributions are

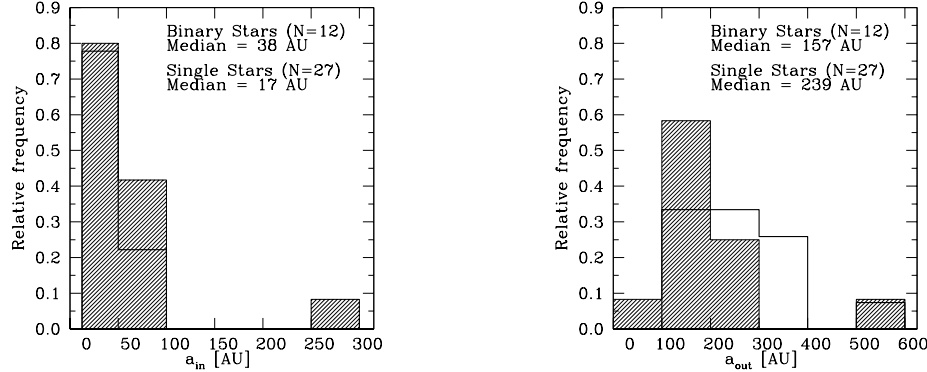


Fig. 2. Left panel: Inner radii distributions for the debris disks in single (empty histogram) and binary systems (dashed histogram). Right panel: Outer radii distributions for our samples of disks in single and binary stars.

drawn from the same population. Consequently, no significant difference between the two distributions was found. Debris disks in both types of stars appear to have been cleared of dust in the inner region ( $\lesssim 3\text{-}5$  AU). None of the systems had emission excesses at  $\lambda < 24 \mu\text{m}$ . This may be an evolutionary effect: gas and dust depletion starts from inside out as the central star evolves (Chen et al. 2005). Considering the ages of the stars in our samples ( $> 100$  Myr), this may explain the relative lack of dust in the inner zone of the disks (Vican & Schneider 2014).

Outer radii distributions are shown in the right panel of Figure 2. The medians are 239 and 157 AU for the disks in single and binary systems, respectively. The probability for both distributions to represent the same population of disks is 0.1 and thus there are no clear differences between them.

Twenty stars in our samples had disk radii estimates in the literature: HD 1404 from (Thureau et al. 2014), HD 10647, HD 13161, HD 23484, HD 27290, HD 48682, HD 102647, HD 104860, HD 109085, HD 170773, HD 172167, HD 195627, HD 207129 and HD 216956 from (Pawellek et al. 2014), HD 17925, HD 20807, HD 30495, HD 90089, HD 110897 and HD 199260 from (Eiroa et al. 2013). In general, these radii were smaller than our determinations. It is known that blackbody models for the dust emission tend to underestimate the radius of the disks. Rodriguez & Zuckerman (2012) found that radii measured from thermally resolved disks were larger by a factor 1 to 5 when compared with those derived from blackbody-fits. Booth et al. (2013) constrained this factor from 1 to 2.5. On average, our radii are a factor between 2.5 to 5 larger than those in the literature. This may explain, at least in part, the differences between Eiroa's and Thureau's esti-

mations. Radii from Pawellek et al. (2014) were derived from PACS/Herschel images at  $\lambda = 70, 100$  or  $160 \mu\text{m}$ . In this case, the difference may be due to the fact that our determinations include fluxes in a wider spectral range and thus our values are weighted by contributions at different wavelengths.

It has been argued that the proximity of a companion star may limit the amount of dust located towards the outer portion of the disk. Depending on the orbit eccentricity and on the mass ratio between components, theoretical studies predict that the outer radius of a disk around the primary star is about  $0.4\text{-}0.5A_{\text{bin}}$  (Artymowicz & Lubow 1994). Nine out of 12 binaries with circumprimary disks have  $a_{out} < 0.4A_{\text{bin}}$  and therefore, the dust is located in a stable zone. The three stars that do not meet this condition are: HD 1404 ( $A_{\text{bin}} = 272$  AU,  $a_{out} = 250$  AU), HD 19994 ( $A_{\text{bin}} = 154$  AU,  $a_{out} = 200$  AU) and HD 91312 ( $A_{\text{bin}} = 585$  AU,  $a_{out} = 570$  AU). In these cases, dust may be located in an unstable zone.

In Table 4 we list binary stars with thermal emission or scatter light resolved debris disks from the literature. This table provides the measured radii ( $a_{\text{res}}$ ), the separations between the components ( $A_{\text{bin}}$ ), and the stability classification according to the criteria from Artymowicz & Lubow (1994). The first six systems in Table 4 are included in our sample of binary stars. We are not considering HD 13161 as it probably has a circumbinary disk. For HD 19994, the radius measured from resolved images places the dust in the unstable region, in agreement with our estimation from the SED modeling. In addition, Rodriguez et al. (2015) also reported that HD 19994 may have the disk in an unstable region. The remaining five systems have the disk in a stable region.

TABLE 4  
BINARY STARS WITH RESOLVED DEBRIS DISKS

| HD                  | $a_{\text{res}}$<br>(AU) | $A_{\text{bin}}$<br>(AU) | Stable? | References              |
|---------------------|--------------------------|--------------------------|---------|-------------------------|
| 19994 <sup>a</sup>  | 95                       | 154                      | No      | Eiroa et al. (2013)     |
| 20807 <sup>a</sup>  | 48                       | 3708                     | Yes     | Eiroa et al. (2013)     |
| 48682 <sup>a</sup>  | 142                      | 598                      | Yes     | Pawellek et al. (2014)  |
| 102647 <sup>a</sup> | 48                       | 433                      | Yes     | Pawellek et al. (2014)  |
| 207129 <sup>a</sup> | 148                      | 858                      | Yes     | Pawellek et al. (2014)  |
| 216956 <sup>a</sup> | 123                      | 54401                    | Yes     | Pawellek et al. (2014)  |
| 13161 <sup>b</sup>  | 161                      | 0.4                      | Yes     | Booth et al. (2013)     |
| 20320 <sup>b</sup>  | 178                      | 0.2 <sup>c</sup>         | Yes     | Booth et al. (2013)     |
| 109573              | 70                       | 502 <sup>d</sup>         | Yes     | Schneider et al. (1999) |
| 139006 <sup>b</sup> | 77                       | 0.2 <sup>c</sup>         | Yes     | Booth et al. (2013)     |
| 181296              | 24                       | 199 <sup>c</sup>         | Yes     | Smith et al. (2009)     |
| 211415              | 100                      | 69 <sup>e</sup>          | No      | Eiroa et al. (2010)     |

<sup>a</sup>In our sample of binary stars.

<sup>b</sup>Likely, circumbinary disks.

<sup>c</sup>Rodriguez & Zuckerman (2012).

<sup>d</sup>Catalog of Components of Double & Multiple stars (on-line version at: <http://vizier.u-strasbg.fr/viz-bin/VizieR-3?-source=I/274/ccdm>).

<sup>e</sup>Tokovinin (2014).

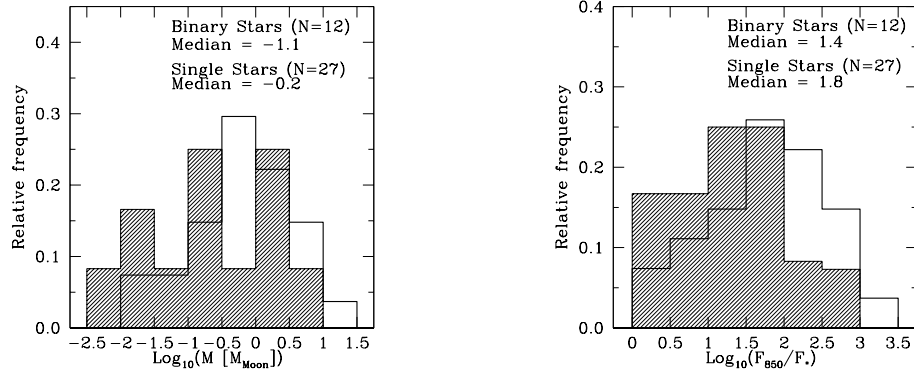


Fig. 3. Left panel: Mass distributions for the disks in single (empty histogram) and binary systems (dashed histogram). Right panel: Flux ratios distributions for single and binary stars at  $\lambda = 850 \mu\text{m}$ .

For HD 1404 and HD 91312 we found no previous reported radii from resolved images. The availability of these images would help to confirm if the dust is located in an unstable zone.

HD 13161, HD 20320 and HD 139006 probably have circumbinary disks because of the small separation between the components. These stars as well as HD 109573 and HD 181296, with likely circumstellar disks, have dust in a stable region. On the

other hand, HD 211415 may have dust in an unstable zone according to the radius determined from resolved images.

### 3.2. Dust Mass and Grain Sizes

Histograms of the dust masses are shown in the left panel of Figure 3. Median values of dust masses for the disks in single and binary stars are  $\approx 0.6$

and  $\approx 0.2 M_{\text{Moon}}$ , respectively. According to the K-S test, the mass distributions do not differ significantly (p-value  $\approx 0.3$ ).

Eight stars in our sample have previous determinations of mass published in the literature including fluxes at  $\lambda > 100 \mu\text{m}$ . Panić et al. (2013) estimated masses for the disks of HD 377 ( $\approx 3.6 M_{\text{Moon}}$ ), HD 92945 ( $\approx 2.1 M_{\text{Moon}}$ ), and HD 115617 ( $\approx 0.2 M_{\text{Moon}}$ ). Thureau et al. (2014) obtained lower limits for the masses of the disks of HD 1404 ( $\approx 0.1 M_{\text{Moon}}$ ), HD 13161 ( $\approx 0.6 M_{\text{Moon}}$ ), HD 102647 ( $\approx 0.01 M_{\text{Moon}}$ ), HD 172167 ( $\approx 0.7 M_{\text{Moon}}$ ) and HD 216956 ( $\approx 0.2 M_{\text{Moon}}$ ). A direct comparison is difficult because of the variety of models applied. The masses from Panić et al. (2013) are, in general, larger than the masses presented here. The difference may arise because the authors used minimum temperatures in their calculations. The masses derived by Thureau et al. (2014) are consistent with our estimations, considering the uncertainties.

The fractional infrared luminosity  $f = L_{\text{IR}}/L_{\text{bol}}$  ( $L_{\text{IR}}$  is the bolometric luminosity of a blackbody disk model, and  $L_{\text{bol}}$  is the bolometric luminosity of the stellar model), has been used in the literature to investigate whether debris disks around single stars are more massive than the disks in binary stars. Thureau et al. (2014) compared  $f$  for 12 single and 9 multiple systems, and though the median value was almost twice as high for single stars, the difference was not significant. A similar trend was presented by Rodriguez & Zuckerman (2012). Rodriguez et al. (2015) also compared fractional luminosities for 55 single stars and 21 binary systems and no difference was reported between the two samples.

Observations of the near-IR and submillimeter emissions for pre-main sequence binary systems suggest smaller emission excesses in comparison with single stars (Jensen et al. 1996; Mathieu et al. 2000; Andrews & Williams 2005; Cieza et al. 2009; Harris et al. 2012). Rieke et al. (2005) analyzed the emission excesses at  $\lambda = 24 \mu\text{m}$  of a sample of 266 main-sequence stars, including about a dozen binary stars. They noticed that emission excess in binaries was smaller than in single stars.

In light of previous results, we inspected the flux ratios of the observed ( $F_{850}$ ) and the stellar ( $F_*$ ) fluxes, as a way to investigate the influence that the cold dust ( $T < 20 \text{ K}$ ) may have in the total mass of the disks. These ratios are listed in Table 3. For systems with no data at  $\lambda = 850 \mu\text{m}$ , we adopted the values predicted by the SEDs models. Figure 3 shows the histograms of the flux ratios. The medians

are 72 and 29 for the single and binary samples. The p-value from K-S test is 0.07 and no significant difference can be claimed, although a marginal trend may be present (see Figure 3, right panel). If confirmed, this marginal trend may indicate a larger amount of cold dust contained in debris disks around single stars. This would be consistent with the notion that the presence of cold dust away from the central star may be restricted by the companion in binary stars. This analysis highlights the need for data on binaries with fluxes at  $\lambda > 100 \mu\text{m}$ .

For  $D_{\min}$ , medians were 9 and  $12 \mu\text{m}$  for single and binary stars with a probability 0.06 of both distributions being drawn from the same sample. For  $D_{\max}$ , medians were 300 and  $265 \mu\text{m}$ , respectively. The K-S test probability is 0.9. No significant difference in grain sizes for the disks in single and binary stars was found from our SEDs modeling. A more detailed and specific mid-IR spectroscopic study could shed some light on this aspect. The shape and features present in the spectra are reliable tracers of the size, structure and chemical composition of the dust grains (for example, the case of  $\beta$  Pictoris, Li et al. 2012).

Several authors have compared the characteristics of disks in single stars with those in binary systems that can be classified as tight ( $A_{\text{bin}} < 1 \text{ AU}$ ) and wide ( $A_{\text{bin}} > 100 \text{ AU}$ ) (see, for example, Rodriguez & Zuckerman 2012; Eiroa et al. 2013; Thureau et al. 2014; Rodriguez et al. 2015). These studies suggest that there are no significant differences in the major characteristics of the debris disks around single stars when compared to the disks in tight and wide binary systems. The results presented in this work also show similar trends. However, all works analyzing samples of debris disks in binary stars lack systems with intermediate separation ( $A_{\text{bin}} \approx 100 \text{ AU}$ ). In our case, this is clearly due to our selection criteria, but this is not the case in the works cited above. Interestingly, Trilling et al. (2007) suggest that the lack of binaries with intermediate separations among those with debris disks is due to the fact that the dust detected in the *Spitzer* bands (at 24 and  $70 \mu\text{m}$ , with  $T \approx 50\text{-}150 \text{ K}$ ), probably lies in an unstable zone.

#### 4. SUMMARY AND CONCLUSIONS

We compiled from the literature a sample of 25 single and 14 binary stars with debris disks. The selected objects were restricted to those with flux measurements available at  $\lambda > 100 \mu\text{m}$ , and ages  $> 100 \text{ Myr}$ . Previous studies focused on the frequency of disks in single and binary stars (see, for

example, Thureau et al. 2014; Rodriguez et al. 2015), although they were not restricted by the availability of sub-mm fluxes. In this contribution, we analyzed smaller samples, but included fluxes in this spectral range to derive individual disk parameters in a comprehensive manner. We constructed and modeled the observed SEDs using a continuum radiative transfer code from Wolf & Hillenbrand (2003). As a result of the SED modeling we obtained the radii ( $a_{\text{in}}, a_{\text{out}}$ ), the mass of dust ( $M_{\text{dust}}$ ) and particle size ( $D_{\text{min}}, D_{\text{max}}$ ) of the disks in our samples.

We compared the characteristics of the disks in both samples. Our analysis showed no significant differences in the inner and outer radii and therefore, in the extension of the disks of the single and binary stars studied in this paper. Both samples of disks were depleted of dust inside 3 - 5 AU and the disks seemed to extend beyond 100 AU, though the median value of outer disk radii in single stars was higher than that of disks in binary systems. The dust masses and emission excesses at  $\lambda = 850 \mu\text{m}$  were comparable for the debris disks in single and binary stars. Our comparison showed that the size of the dust that populates the debris disks in single

and binary systems is similar. However, a more careful and detailed spectroscopy study would be needed to better address this issue.

Although the analyzed samples of single and binary stars are modest, our modeling provides radii, masses, and dust size estimates for 39 debris disks around *FGK* type stars using very well sampled SEDs, particularly at long wavelengths. To further improve the analysis of this paper and to confirm the trends found here it is essential to increase the number of observations of stars with debris disk, particularly in the submillimeter range, and for binary stars. In that sense, instruments such as ALMA will allow a great progress in the coming years.

We wish to thank the anonymous referee for the constructive suggestions that helped us to improve the content of the paper and to clarify our results.

## APPENDICES

### A. TABLES WITH THE FLUXES USED TO CONSTRUCT THE OBSERVED SEDs

TABLE 5  
FLUXES AT  $\lambda > 22 \mu\text{m}$  USED TO CONSTRUCT THE OBSERVED SEDs FOR SINGLE STARS

| Source (HD)                     | Flux [mJy]                  |                           |                             |                             |                            |                            |                             |                             |                           |                           |                             |                           |                           |                           |                  |                          |                  |                  |
|---------------------------------|-----------------------------|---------------------------|-----------------------------|-----------------------------|----------------------------|----------------------------|-----------------------------|-----------------------------|---------------------------|---------------------------|-----------------------------|---------------------------|---------------------------|---------------------------|------------------|--------------------------|------------------|------------------|
|                                 | 24                          | MIPS<br>70                | 160                         | IRS<br>31                   | 25                         | IRAS<br>60                 | 100                         | AKARI<br>90                 | 70                        | PACS<br>100               | 160                         | 250                       | SPIRE<br>350              | 500                       | 450              | 850                      | SCUBA            | LABOCA<br>870    |
| Wavelength<br>[ $\mu\text{m}$ ] |                             |                           |                             |                             |                            |                            |                             |                             |                           |                           |                             |                           |                           |                           |                  |                          |                  |                  |
| 377                             | 38.2 $\pm$ 0.8 <sup>a</sup> | 162 $\pm$ 13 <sup>a</sup> | 187 $\pm$ 50 <sup>b</sup>   | 39.1 $\pm$ 2.9 <sup>a</sup> | ... <sup>c</sup>           | <179 <sup>c</sup>          | <272 <sup>c</sup>           | 270 $\pm$ 18 <sup>c</sup> * | ... <sup>c</sup>          | ... <sup>c</sup>          | ... <sup>c</sup>            | ... <sup>c</sup>          | ... <sup>c</sup>          | ... <sup>c</sup>          | ... <sup>c</sup> | <36d                     | 4.6 $\pm$ 1.2d   |                  |
| 8907                            | 51.3 $\pm$ 2.1 <sup>a</sup> | 247 $\pm$ 9 <sup>a</sup>  | 244 $\pm$ 42 <sup>b</sup>   | 41.9 $\pm$ 4.5 <sup>a</sup> | 1.12 $\pm$ 27 <sup>c</sup> | 285 $\pm$ 4 <sup>c</sup>   | 81.5 $\pm$ 106 <sup>i</sup> | 1030 $\pm$ 170 <sup>j</sup> | 904 $\pm$ 65 <sup>k</sup> | 863 $\pm$ 59 <sup>h</sup> | 813 $\pm$ 80 <sup>l</sup>   | 636 $\pm$ 32 <sup>m</sup> | 312 $\pm$ 26 <sup>n</sup> | 180 $\pm$ 15 <sup>m</sup> | ... <sup>c</sup> | 22 $\pm$ 11 <sup>g</sup> | 4.8 $\pm$ 1.2g   |                  |
| 10647                           | 185 $\pm$ 4 <sup>i</sup>    | ... <sup>c</sup>          | 185 $\pm$ 7 <sup>a</sup>    | 282 $\pm$ 37 <sup>i</sup>   | 8.15 $\pm$ 37 <sup>i</sup> | 149 $\pm$ 40 <sup>j</sup>  | ... <sup>c</sup>            | ... <sup>c</sup>            | 68 $\pm$ 8 <sup>h</sup>   | 48.5 $\pm$ 3 <sup>j</sup> | 75 $\pm$ 2.7 <sup>h</sup>   | 91.9 $\pm$ 4.9m           | 53.0 $\pm$ 10.4m          | 32.2 $\pm$ 8.9m           | <21.6m           | ... <sup>c</sup>         | <78              |                  |
| 17925                           | 184 $\pm$ 4 <sup>h</sup>    | ... <sup>c</sup>          | 185 $\pm$ 42 <sup>i</sup>   | 426 $\pm$ 42 <sup>i</sup>   | 1.18 $\pm$ 19 <sup>i</sup> | 1.36 $\pm$ 33 <sup>i</sup> | ... <sup>c</sup>            | ... <sup>c</sup>            | 88.5 $\pm$ 7.5h           | 75 $\pm$ 2.7 <sup>h</sup> | 134.3 $\pm$ 14.1m           | 52.5 $\pm$ 6.5m           | 23.5 $\pm$ 8m             | 14.1 $\pm$ 6.9h           | <16.7m           | ... <sup>c</sup>         | ... <sup>c</sup> |                  |
| 23484                           | 75.9 $\pm$ 1.6 <sup>h</sup> | ... <sup>c</sup>          | 50.7 $\pm$ 3.2 <sup>a</sup> | 1.18 $\pm$ 19 <sup>i</sup>  | 205 $\pm$ 33 <sup>c</sup>  | 428 $\pm$ 26 <sup>c</sup>  | 205 $\pm$ 49 <sup>i</sup>   | 205 $\pm$ 49 <sup>i</sup>   | 220 $\pm$ 6 <sup>l</sup>  | 184 $\pm$ 4 <sup>l</sup>  | 114 $\pm$ 9 <sup>h</sup>    | 80.0 $\pm$ 5.2h           | 23.2 $\pm$ 6.8h           | 14.1 $\pm$ 6.9h           | <28.8h           | ... <sup>c</sup>         | ... <sup>c</sup> |                  |
| 27290                           | 316 $\pm$ 3 <sup>l</sup>    | ... <sup>c</sup>          | 128 $\pm$ 18 <sup>a</sup>   | 224 $\pm$ 27 <sup>i</sup>   | 12.8 $\pm$ 8 <sup>a</sup>  | 242 $\pm$ 49 <sup>i</sup>  | ... <sup>c</sup>            | ... <sup>c</sup>            | ... <sup>c</sup>          | ... <sup>c</sup>          | ... <sup>c</sup>            | ... <sup>c</sup>          | ... <sup>c</sup>          | ... <sup>c</sup>          | ... <sup>c</sup> | ... <sup>c</sup>         | ... <sup>c</sup> |                  |
| 30495                           | 201 $\pm$ 4 <sup>a</sup>    | ... <sup>c</sup>          | 620 $\pm$ 11 <sup>a</sup>   | ... <sup>c</sup>            | 98 $\pm$ 3a                | 613 $\pm$ 47 <sup>n</sup>  | 404 $\pm$ 88e <sup>o</sup>  | ... <sup>c</sup>            | ... <sup>c</sup>          | ... <sup>c</sup>          | ... <sup>c</sup>            | ... <sup>c</sup>          | 502 $\pm$ 160P            | ... <sup>c</sup>          | 93 $\pm$ 239     | ... <sup>c</sup>         | ... <sup>c</sup> |                  |
| 61005                           | 42 $\pm$ 1 <sup>a</sup>     | ... <sup>c</sup>          | 90089                       | 149 $\pm$ 1 <sup>l</sup>    | ... <sup>c</sup>           | 201 $\pm$ 20 <sup>i</sup>  | 145 $\pm$ 29 <sup>j</sup>   | 540 $\pm$ 103 <sup>i</sup>  | ... <sup>c</sup>          | 39.6 $\pm$ 3.8h           | 46.7 $\pm$ 2.8 <sup>l</sup> | ... <sup>c</sup>          | 49.6 $\pm$ 8.3h           | 41.0 $\pm$ 8.1h           | 23.1 $\pm$ 9.4h  | ... <sup>c</sup>         | ... <sup>c</sup> |                  |
| 92945                           | 39 $\pm$ 1 <sup>a</sup>     | 305 $\pm$ 15 <sup>a</sup> | 285 $\pm$ 34 <sup>r</sup>   | 274 $\pm$ 4 <sup>a</sup>    | 16 $\pm$ 3a                | 248 $\pm$ 45 <sup>i</sup>  | 982 $\pm$ 295 <sup>i</sup>  | ... <sup>c</sup>            | ... <sup>c</sup>          | 277 $\pm$ 4m              | 243 $\pm$ 5m                | ... <sup>c</sup>          | 50 $\pm$ 15m              | ... <sup>c</sup>          | ... <sup>c</sup> | <120d                    | 9 $\pm$ 1d       |                  |
| 104860                          | 20.0 $\pm$ 0.4 <sup>a</sup> | 183 $\pm$ 7 <sup>a</sup>  | 669 $\pm$ 10 <sup>a</sup>   | 81 $\pm$ 6 <sup>a</sup>     | 602 $\pm$ 34a              | 770 $\pm$ 62 <sup>i</sup>  | 910 $\pm$ 155e              | 556 $\pm$ 65s               | ... <sup>c</sup>          | 259 $\pm$ 4 <sup>l</sup>  | 300 $\pm$ 30 <sup>l</sup>   | 231 $\pm$ 13n             | ... <sup>c</sup>          | ... <sup>c</sup>          | 47 $\pm$ 14m     | 6.8 $\pm$ 1.2m           | ... <sup>c</sup> |                  |
| 107146                          | 543 $\pm$ 11t               | ... <sup>c</sup>          | 110897                      | 111.1 $\pm$ 2h              | 666 $\pm$ 3a               | 159 $\pm$ 43 <sup>e</sup>  | <172 <sup>e</sup>           | ... <sup>c</sup>            | 56.5 $\pm$ 5h             | 47 $\pm$ 3 <sup>l</sup>   | 47 $\pm$ 3 <sup>l</sup>     | 43.9 $\pm$ 3.2u           | ... <sup>c</sup>          | ... <sup>c</sup>          | 231 $\pm$ 13n    | 15.5 $\pm$ 1.4m          | ... <sup>c</sup> |                  |
| 1109085                         | 115617                      | 458 $\pm$ 5 <sup>l</sup>  | 128167                      | 56 $\pm$ 12w <sup>*</sup>   | 268 $\pm$ 5 <sup>a</sup>   | 172 $\pm$ 2x <sup>w</sup>  | 37.6 $\pm$ 49 <sup>n</sup>  | 140 $\pm$ 35 <sup>i</sup>   | ... <sup>c</sup>          | 156 $\pm$ 8 <sup>l</sup>  | 152 $\pm$ 6 <sup>l</sup>    | 133 $\pm$ 6v              | ... <sup>c</sup>          | ... <sup>c</sup>          | 58 $\pm$ 10m     | 15.5 $\pm$ 1.4m          | ... <sup>c</sup> |                  |
| 128167                          | 139664                      | 263 $\pm$ 5 <sup>t</sup>  | 504 $\pm$ 9 <sup>a</sup>    | <1710z <sup>akira</sup>     | 212 $\pm$ 7 <sup>x</sup>   | 693 $\pm$ 125 <sup>n</sup> | 661 $\pm$ 60n               | ... <sup>c</sup>            | 542 $\pm$ 16z             | ... <sup>c</sup>          | 29.6 $\pm$ 4 <sup>l</sup>   | ... <sup>c</sup>          | ... <sup>c</sup>          | ... <sup>c</sup>          | ... <sup>c</sup> | 6 $\pm$ 2y               | ... <sup>c</sup> |                  |
| 145229                          | 32 $\pm$ 1 <sup>a</sup>     | 64 $\pm$ 7a               | 34 $\pm$ 25b                | 25 $\pm$ 2a                 | ... <sup>c</sup>           | 54.9 $\pm$ 2.3a            | 788 $\pm$ 56 <sup>a</sup>   | ... <sup>c</sup>            | 575 $\pm$ 32n             | <1030 <sup>c</sup>        | ... <sup>c</sup>            | ... <sup>c</sup>          | ... <sup>c</sup>          | ... <sup>c</sup>          | ... <sup>c</sup> | ... <sup>c</sup>         | 18.0 $\pm$ 5.4m  |                  |
| 170773                          | 67.0 $\pm$ 1.4 <sup>a</sup> | 11400 $\pm$ 90ab          | 172167                      | 11.300 $\pm$ 600ab          | 951.0 $\pm$ 760ab          | 7760 $\pm$ 709ab           | 6200 $\pm$ 170k             | ... <sup>c</sup>            | ... <sup>c</sup>          | 4610 $\pm$ 900m           | 1680 $\pm$ 260m             | 610 $\pm$ 100m            | 210 $\pm$ 40m             | ... <sup>c</sup>          | 46 $\pm$ 5m      | ... <sup>c</sup>         | ... <sup>c</sup> |                  |
| 191089                          | 181 $\pm$ t                 | 54.4 $\pm$ 13a            | 205 $\pm$ 45b               | 354 $\pm$ 10 <sup>a</sup>   | 159 $\pm$ 5 <sup>a</sup>   | 264 $\pm$ 32 <sup>i</sup>  | 711.5 $\pm$ 57i             | 1.95 $\pm$ 106 <sup>o</sup> | 586 $\pm$ 45k             | ... <sup>c</sup>          | 607.9 $\pm$ 43.5m           | 405.4 $\pm$ 29.3m         | 145.9 $\pm$ 14.1m         | 70.9 $\pm$ 7.7m           | 34.1 $\pm$ 7.5m  | ... <sup>c</sup>         | 13 $\pm$ 7m      | ... <sup>c</sup> |
| 195627                          | 207 $\pm$ 4 <sup>a</sup>    | 609 $\pm$ 61a             | 120 $\pm$ 4 <sup>a</sup>    | 73 $\pm$ 2a                 | ... <sup>c</sup>           | 15.5 $\pm$ 4 <sup>a</sup>  | ... <sup>c</sup>            | ... <sup>c</sup>            | 45 $\pm$ 2 <sup>l</sup>   | 23 $\pm$ 3 <sup>l</sup>   | 8 $\pm$ 2h                  | ... <sup>c</sup>          | ... <sup>c</sup>          | ... <sup>c</sup>          | ... <sup>c</sup> | ... <sup>c</sup>         | ... <sup>c</sup> |                  |
| 199260                          | 22.7 $\pm$ 0.5 <sup>a</sup> | 42 $\pm$ 7 <sup>a</sup>   | 90 $\pm$ 42b                | 18.7 $\pm$ 3.5a             | 15.5 $\pm$ 4 <sup>a</sup>  | 158 $\pm$ 44 <sup>i</sup>  | 143 $\pm$ 42 <sup>i</sup>   | ... <sup>c</sup>            | ... <sup>c</sup>          | ... <sup>c</sup>          | ... <sup>c</sup>            | ... <sup>c</sup>          | ... <sup>c</sup>          | ... <sup>c</sup>          | ... <sup>c</sup> | ... <sup>c</sup>         | ... <sup>c</sup> |                  |
| 212695                          | 33.3 $\pm$ 3.6a             | 38 $\pm$ 3.7 <sup>a</sup> | ... <sup>c</sup>            | 18.7 $\pm$ 3.5a             | 158 $\pm$ 44 <sup>i</sup>  | 143 $\pm$ 42 <sup>i</sup>  | ... <sup>c</sup>            | ... <sup>c</sup>            | ... <sup>c</sup>          | ... <sup>c</sup>          | ... <sup>c</sup>            | ... <sup>c</sup>          | ... <sup>c</sup>          | ... <sup>c</sup>          | ... <sup>c</sup> | ... <sup>c</sup>         | ... <sup>c</sup> |                  |
|                                 |                             |                           |                             |                             |                            |                            |                             |                             |                           |                           |                             |                           |                           |                           |                  |                          |                  |                  |

<sup>a</sup>Chen et al. (2014), <sup>b</sup>Hillenbrand et al. (2008), <sup>c</sup>Egan & Price (1996), <sup>d</sup>Panić et al. (2013), <sup>e</sup>Abrahamyan et al. (2015), <sup>f</sup>Moór et al. (2006), <sup>g</sup>Najita & Williams (2005), <sup>h</sup>Eiroa et al. (2013), <sup>i</sup>Moshir & et al. (1990), <sup>j</sup>de Grijp et al. (1992), <sup>k</sup>Ishihara et al. (2010), <sup>l</sup>Gáspár et al. (2014), <sup>m</sup>Pawellek et al. (2013), <sup>n</sup>Helou & Walker (1988), <sup>o</sup>Saunders et al. (2000), <sup>p</sup>Steele et al. (2015), <sup>q</sup>Roccatagliata et al. (2009), <sup>r</sup>Golimowski et al. (2011), <sup>s</sup>Liu et al. (2014), <sup>t</sup>Mizusawa et al. (2012), <sup>u</sup>Marshall et al. (2014), <sup>v</sup>Wyatt et al. (2012), <sup>w</sup>Habing et al. (2001), <sup>x</sup>Chen et al. (2006), <sup>y</sup>Nilsson et al. (2010), <sup>z</sup>Yamamura et al. (2010), <sup>aa</sup>Su et al. (2006), <sup>ab</sup>Hindsley & Harrington (1994), <sup>ac</sup>Carpenter et al. (2008), <sup>ad</sup>Beichman et al. (2006), <sup>ae</sup>Thureau et al. (2013), <sup>ag</sup>Bulger et al. (2011), <sup>ah</sup>Di Francesco et al. (2008), <sup>ai</sup>Shere et al. (2014).

\*Data from the ISO mission.

\*\* Data from the AKARI mission.

TABLE 6  
FLUXES AT  $\lambda > 22 \mu\text{m}$  USED TO CONSTRUCT THE OBSERVED SEDS FOR BINARY STARS

| Source (HD)<br>Wavelength<br>[ $\mu\text{m}$ ] | Flux [mJy]                 |                           |                           |                            |                             |                             |                             |                             |                             |                             |
|--|----------------------------|---------------------------|---------------------------|----------------------------|-----------------------------|-----------------------------|-----------------------------|-----------------------------|-----------------------------|-----------------------------|
|  | 24                         | 70                        | 160                       | 31                         | 25                          | IRAS<br>60                  | 100                         | 90                          | 70                          | PACS                        |
| 1404   | 155 $\pm$ 2 <sup>j</sup>   | ...                       | 105 $\pm$ 2 <sup>a</sup>  | 187 $\pm$ 32 <sup>i</sup>  | 154 $\pm$ 48 <sup>i</sup>   | ...                         | ...                         | 43.8 $\pm$ 6.1 <sup>j</sup> | 27.8 $\pm$ 2.7 <sup>j</sup> | 12.9 $\pm$ 4.1 ae           |
| 13161  | 764 $\pm$ 8 <sup>j</sup>   | 643 $\pm$ 51 <sup>a</sup> | ...                       | 61.2 $\pm$ 9 <sup>a</sup>  | 110.0 $\pm$ 90 <sup>n</sup> | 779 $\pm$ 9 <sup>j</sup>    | ...                         | 591 $\pm$ 52 <sup>s</sup>   | 481 $\pm$ 23 <sup>m</sup>   | 263.6 $\pm$ 0.3 m           |
| 19994  | 218 $\pm$ 4 <sup>j</sup>   | ...                       | ...                       | ...                        | 316 $\pm$ 60 <sup>h</sup>   | <232 <sup>e</sup>           | 169 $\pm$ 38 <sup>i</sup>   | 42.5 $\pm$ 4.8 <sup>j</sup> | 32.3 $\pm$ 3.1 <sup>j</sup> | 31.7 $\pm$ 1.9 <sup>u</sup> |
| 20807  | 222 $\pm$ 5 <sup>j</sup>   | ...                       | 130 $\pm$ 17 <sup>a</sup> | 246 $\pm$ 47 <sup>i</sup>  | 169 $\pm$ 43 <sup>i</sup>   | 317 $\pm$ 54 <sup>i</sup>   | 41.7 $\pm$ 3.3 <sup>j</sup> | 37.7 $\pm$ 3 <sup>j</sup>   | 42.6 $\pm$ 2.5 <sup>h</sup> | 59.7 $\pm$ 6.7 <sup>h</sup> |
| 355850   | 83 $\pm$ 3 <sup>a</sup>    | 247 $\pm$ 20 ac           | 244 $\pm$ 42 ac           | 54 $\pm$ 7 <sup>a</sup>    | 80 $\pm$ 23 <sup>35</sup>   | 228 $\pm$ 36 <sup>i</sup>   | 483 $\pm$ 116 <sup>i</sup>  | ...                         | ...                         | ...                         |
| 38393  | <76 <sup>ad</sup>          | ...                       | ...                       | 981 $\pm$ 59 <sup>i</sup>  | ...                         | ...                         | 87 $\pm$ 3 <sup>i</sup>     | 55 $\pm$ 5 <sup>i</sup>     | ...                         | ...                         |
| 48682  | 193 $\pm$ 4 <sup>h</sup>   | ...                       | ...                       | 412 $\pm$ 41 <sup>i</sup>  | 381 $\pm$ 50 <sup>i</sup>   | ...                         | 263 $\pm$ 18 <sup>h</sup>   | 252 $\pm$ 3 <sup>m</sup>    | 182 $\pm$ 4 <sup>m</sup>    | 120 $\pm$ 1.1 m             |
| 91312  | ...                        | ...                       | ...                       | 185 $\pm$ 30 <sup>i</sup>  | 397 $\pm$ 54 <sup>i</sup>   | ...                         | ...                         | <22 <sup>48</sup>           | <34 <sup>ag</sup>           | 25 $\pm$ 8 <sup>m</sup>     |
| 102647   | 1600 $\pm$ 70 <sup>a</sup> | 676 $\pm$ 46 aa           | ...                       | 1240 $\pm$ 10 <sup>a</sup> | 2110 $\pm$ 230 <sup>n</sup> | 1030 $\pm$ 160 <sup>i</sup> | 615 $\pm$ 51 <sup>k</sup>   | 215 $\pm$ 30 <sup>af</sup>  | 51 $\pm$ 12 <sup>af</sup>   | <39 <sup>af</sup>           |
| 139813   | 46 $\pm$ 8 <sup>ac</sup>   | ...                       | ...                       | 123 $\pm$ 21 <sup>n</sup>  | 103 $\pm$ 19 <sup>i</sup>   | 354 $\pm$ 57 <sup>i</sup>   | ...                         | 480 $\pm$ 30 <sup>af</sup>  | ...                         | <15 <sup>af</sup>           |
| 139323   | 43 $\pm$ 3 <sup>a</sup>    | ...                       | 23 $\pm$ 2 <sup>a</sup>   | 70 $\pm$ 15 <sup>e</sup>   | 142 $\pm$ 28 <sup>i</sup>   | 614 $\pm$ 129 <sup>i</sup>  | ...                         | ...                         | ...                         | 130 $\pm$ 12 <sup>g</sup>   |
| 161897   | 30 $\pm$ 3 ac              | <19 ac                    | ...                       | 56 <sup>e</sup>            | 76 $\pm$ 10 <sup>i</sup>    | 406 $\pm$ .9 <sup>i</sup>   | ...                         | ...                         | 234 $\pm$ 68 ag             | ...                         |
| 207129   | 23 $\pm$ 1 <sup>a</sup>    | ...                       | 15 $\pm$ 4 <sup>a</sup>   | ...                        | ...                         | ...                         | ...                         | ...                         | ...                         | 130 $\pm$ 12 <sup>g</sup>   |
| 216056   | 3850 $\pm$ 190 aa          | 9060 $\pm$ 746 aa         | ...                       | 4810 $\pm$ 380 n           | 9030 $\pm$ 11080 n          | 10300 $\pm$ 700 k           | ...                         | 278 $\pm$ 22 <sup>h</sup>   | 311 $\pm$ 1 m               | 44.3 $\pm$ 9 m              |
|  |                            |                           |                           |                            |                             |                             |                             | ...                         | 4660 $\pm$ 1370 k**         | 2700 $\pm$ 300 m            |
|  |                            |                           |                           |                            |                             |                             |                             | ...                         | 500 $\pm$ 50 m              | 595 $\pm$ 35 m              |
|  |                            |                           |                           |                            |                             |                             |                             | ...                         | 500 $\pm$ 100 m             | <70 ah                      |

<sup>a</sup>Chen et al. (2014), <sup>b</sup>Hillenbrand et al. (2008), <sup>c</sup>Egan & Price (1996), <sup>d</sup>Panić et al. (2013), <sup>e</sup>Abrahamyan et al. (2015), <sup>f</sup>Moór et al. (2006), <sup>g</sup>Najita & Williams (2005), <sup>h</sup>Eiroa et al. (2013), <sup>i</sup>Moshir & et al. (1990), <sup>j</sup>de Grijp et al. (1992), <sup>k</sup>Ishihara et al. (2010), <sup>l</sup>Gáspár et al. (2014), <sup>m</sup>Pawellek et al. (2013), <sup>n</sup>Helou & Walker (1988), <sup>o</sup>Saunders et al. (2000), <sup>p</sup>Steede et al. (2015), <sup>q</sup>Roccatagliata et al. (2009), <sup>r</sup>Golimowski et al. (2011), <sup>s</sup>Liu et al. (2014), <sup>t</sup>Mizusawa et al. (2012), <sup>u</sup>Marshall et al. (2014), <sup>v</sup>Wyatt et al. (2012), <sup>w</sup>Habing et al. (2001), <sup>x</sup>Chen et al. (2006), <sup>y</sup>Nilsson et al. (2010), <sup>z</sup>Yamamura et al. (2013), <sup>aa</sup>Su et al. (2006), <sup>ab</sup>Hindsley & Harrington (1994), <sup>ac</sup>Carpenter et al. (2008), <sup>ad</sup>Beichman et al. (2006), <sup>ae</sup>Thureau et al. (2014), <sup>af</sup>Bulger et al. (2013), <sup>ag</sup>Di Francesco et al. (2008), <sup>ai</sup>Sheret et al. (2004).

\*Data from the ISO mission.  
\*\* Data from the AKARI mission.

## B. FULL LIST OF FIGURES OF THE MODELED SEDS

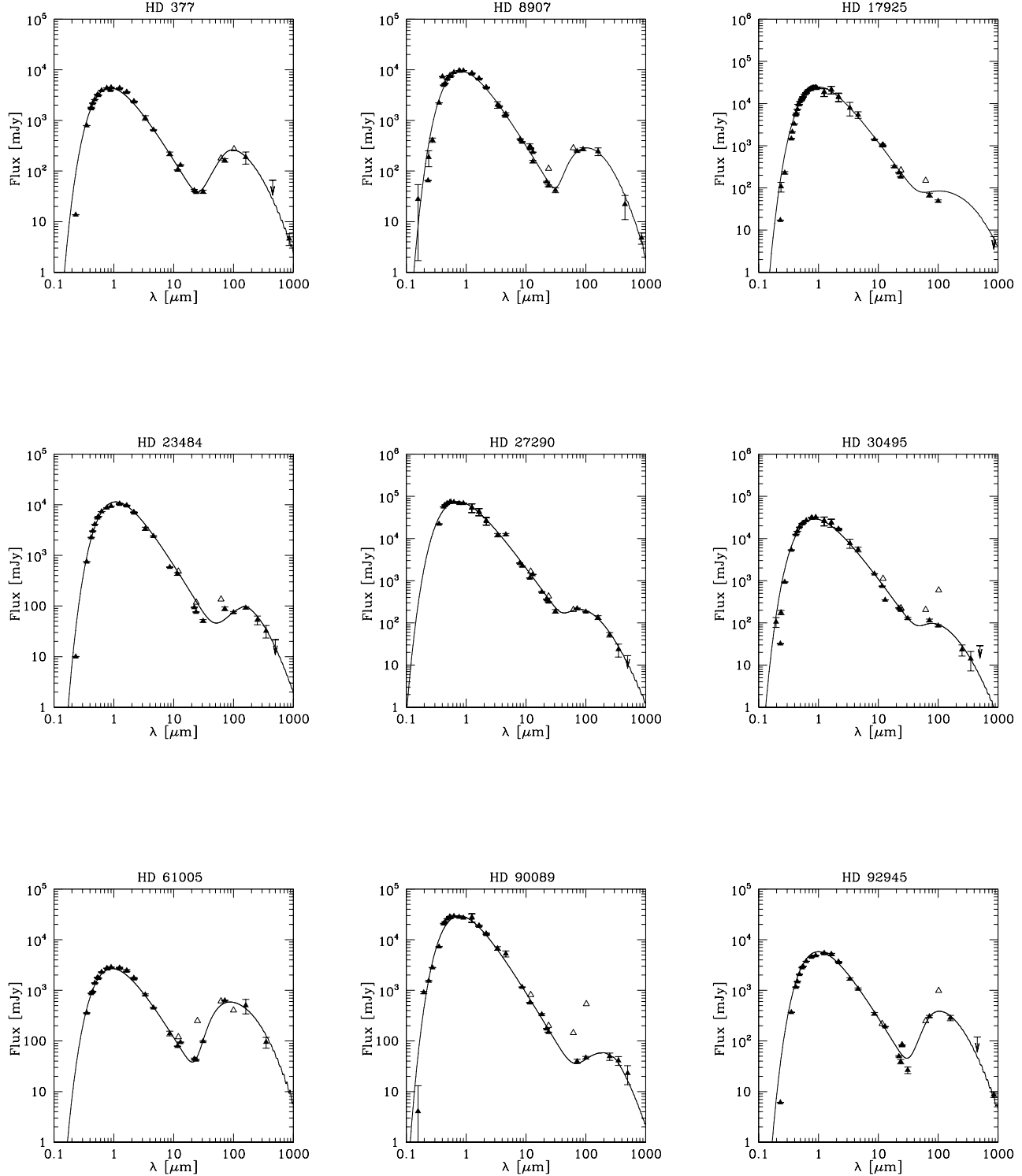


Fig. 4. Model SEDs for the sample of single stars. Triangles indicate actual fluxes and arrows upper limits. Error bars for fluxes at different wavelengths are included. Observations from IRAS are indicated with empty triangles but were not used in the modeling.

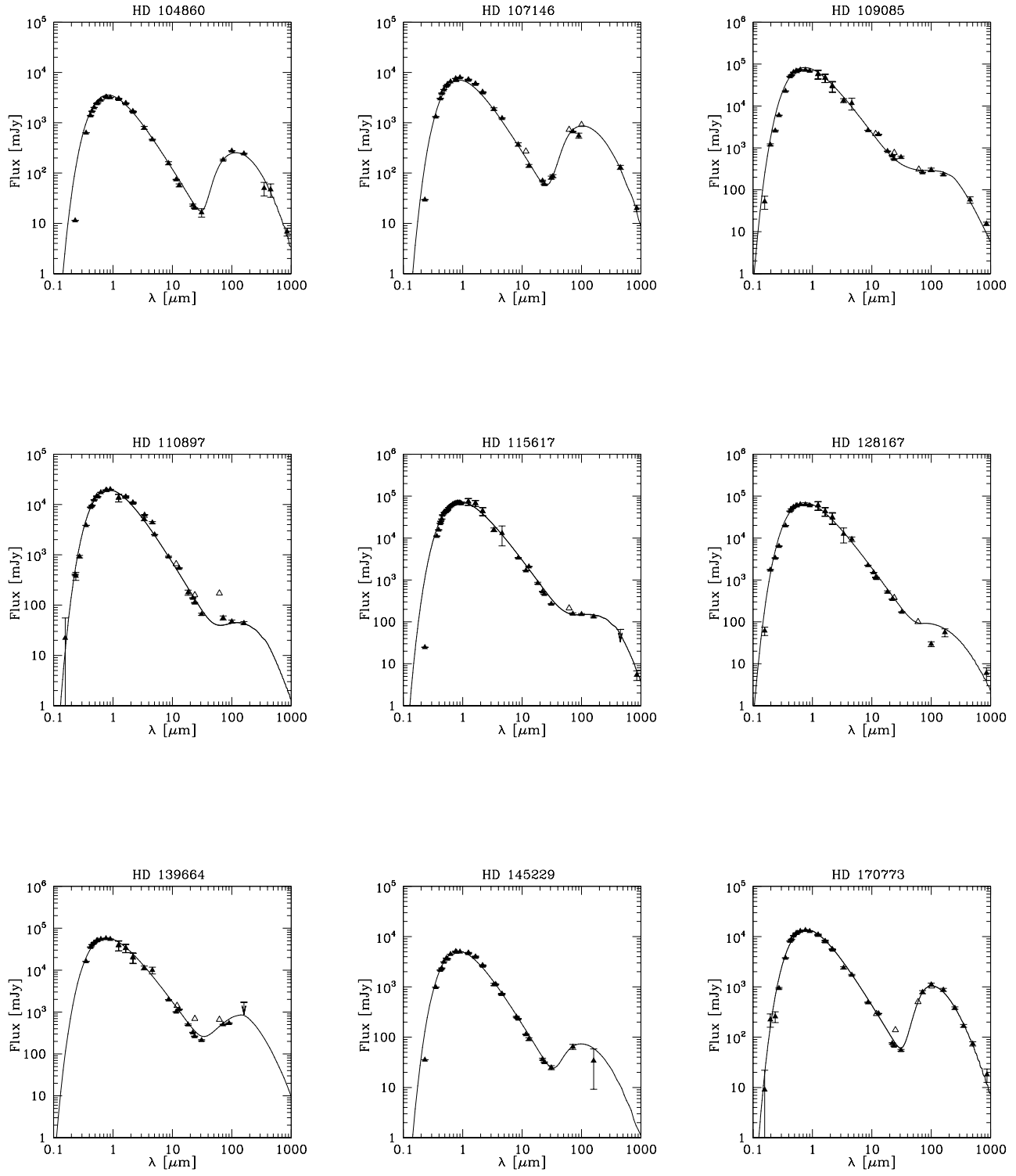


Fig. 4. Continued.

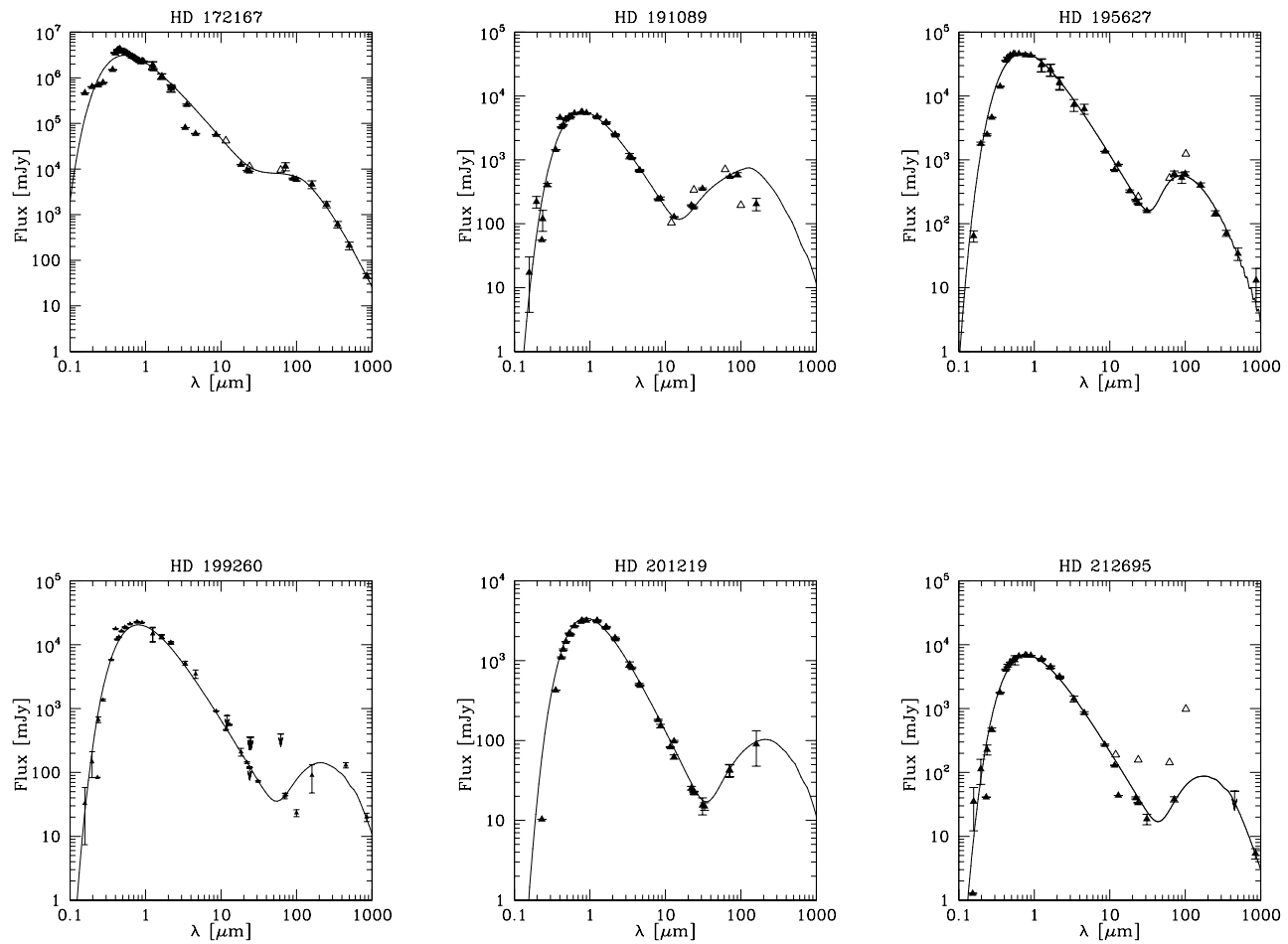


Fig. 4. Continued.

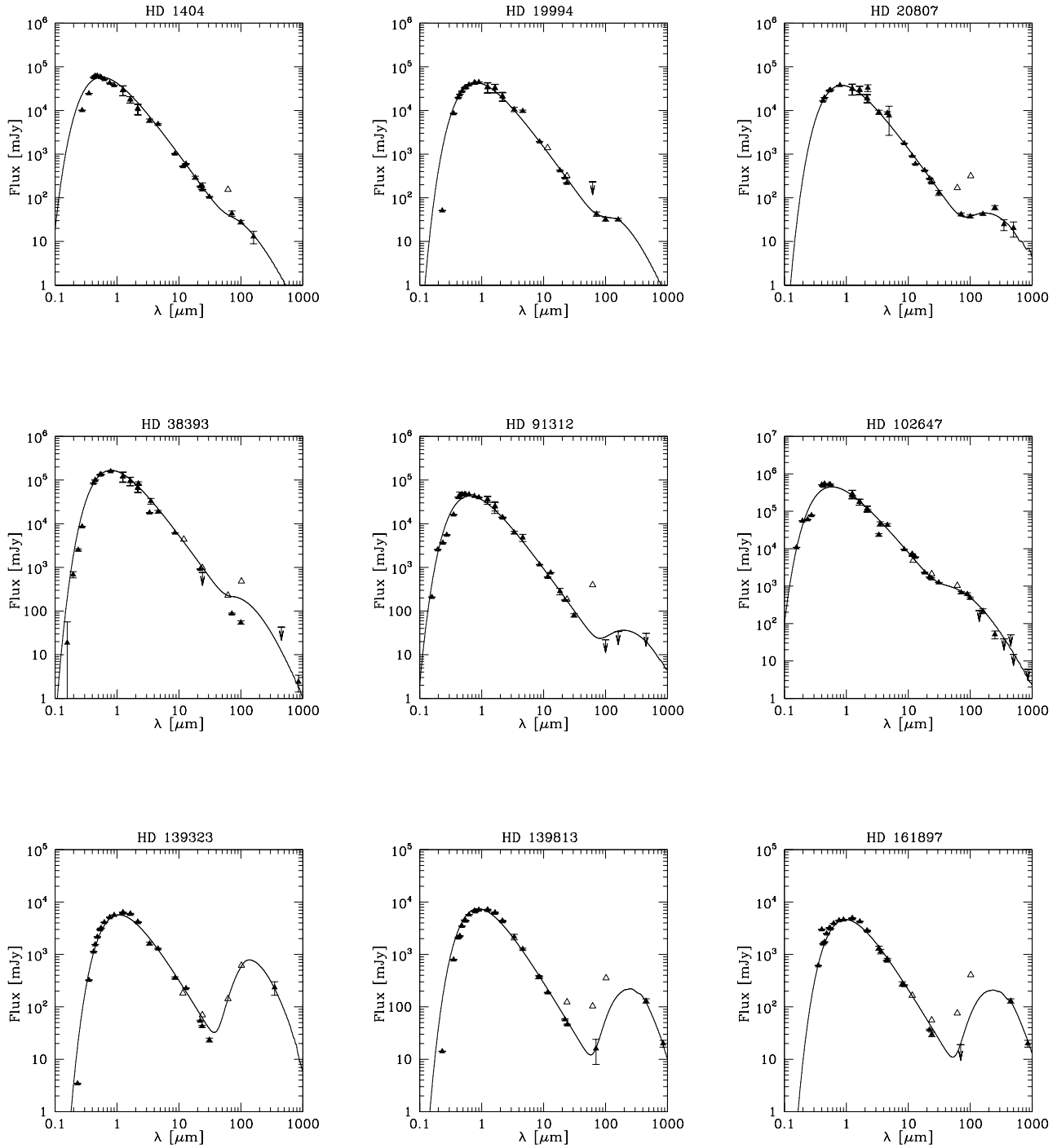


Fig. 5. Model SEDs for the sample of binary stars. Triangles indicate actual fluxes and arrows upper limits. Error bars for fluxes at different wavelengths are included. Observations from IRAS are indicated with empty triangles but were not used in the modeling.

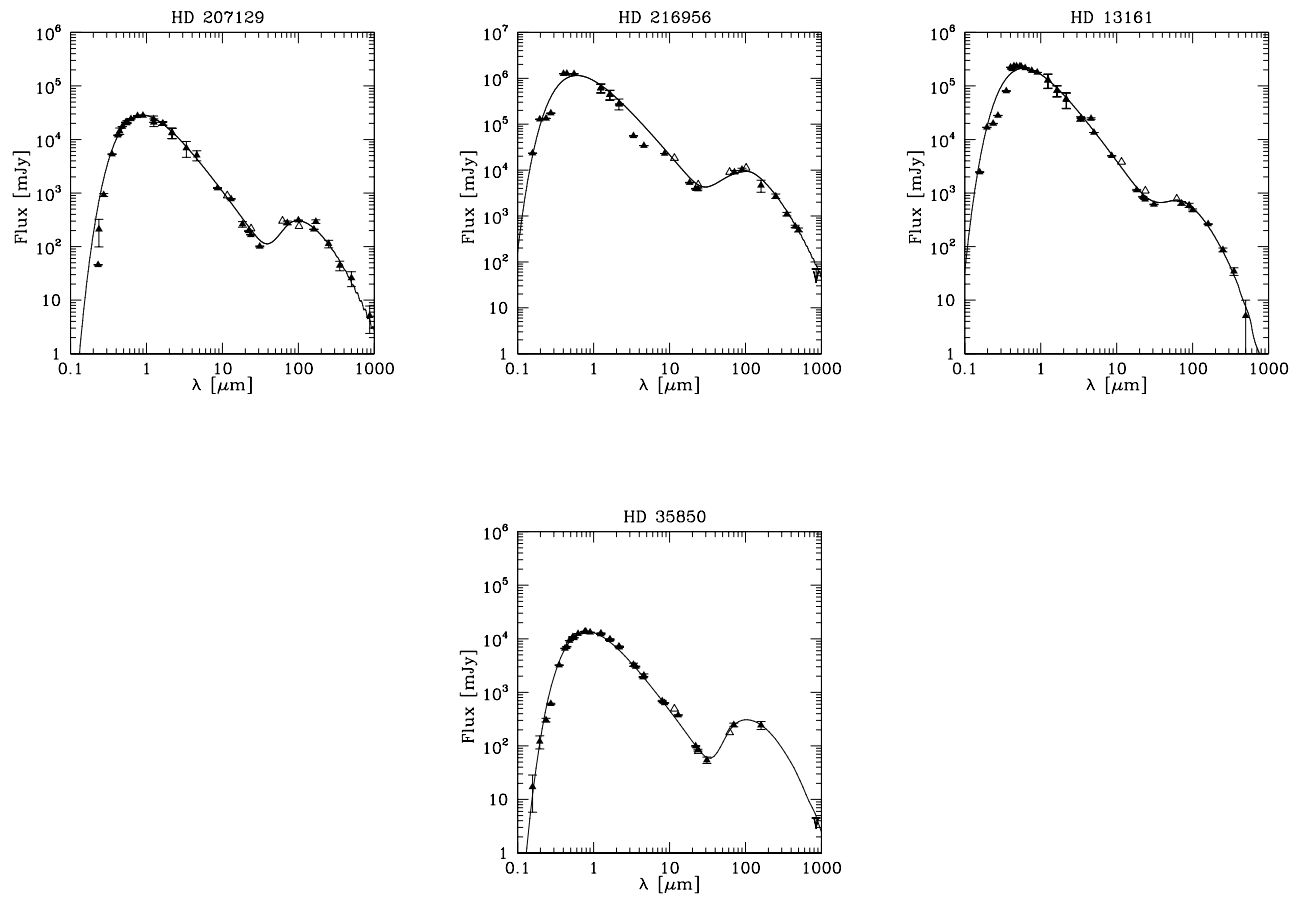


Fig. 5. Continued.

## REFERENCES

- Abrahamyan, H. V., Mickaelian, A. M., & Knyazyan, A. V. 2015, *A&C*, 10, 99
- Andrews, S. M. & Williams, J. P. 2005, *ApJ*, 631, 1134
- Artymowicz, P. & Lubow, S. H. 1994, *ApJ*, 421, 651
- Augereau, J. C., Lagrange, A. M., Mouillet, D., & Ménard, F. 1999, *A&A*, 350, L51
- Aumann, H. H., Beichman, C. A., Gillett, F. C., et al. 1984, *ApJ*, 278, L23
- Backman, D. E. & Paresce, F. 1993, *Protostars and Planets III*, ed. E. H. Levy & J. I. Lunine, (Arizona, A2:UAO) 1253
- Beichman, C. A., Bryden, G., Gautier, T. N., et al. D. 2005a, *ApJ*, 626, 1061
- Beichman, C. A., Bryden, G., Rieke, G. H., et al. 2005b, *ApJ*, 622, 1160
- Beichman, C. A., Bryden, G., Stapelfeldt, K. R., et al. 2006, *ApJ*, 652, 1674
- Booth, M., Kennedy, G., Sibthorpe, B., et al. 2013, *MNRAS*, 428, 1263
- Bryden, G., Beichman, C. A., Trilling, D. E., et al. 2006, *ApJ*, 636, 1098
- Bulger, J., Hufford, T., Schneider, A., et al. 2013, *A&A*, 556, A119
- Carpenter, J. M., Bouwman, J., Mamajek, E. E., et al. 2009, *ApJS*, 181, 197
- Carpenter, J. M., Bouwman, J., Silverstone, M. D., et al. 2008, *ApJS*, 179, 423
- Casagrande, L., Schönrich, R., Asplund, M., Cassisi, S., Ramírez, I., Meléndez, J., Bensby, T., & Feltzing, S. 2011, *A&A*, 530, A138
- Chen, C. H., Li, A., Bohac, C., et al. 2007, *ApJ*, 666, 466
- Chen, C. H., Mittal, T., Kuchner, M., Forrest, W. J., Lisse, C. M., Manoj, P., Sargent, B. A., & Watson, D. M. 2014, *ApJS*, 211, 25
- Chen, C. H., Patten, B. M., Werner, M. W., et al. 2005, *ApJ*, 634, 1372
- Chen, C. H., Sargent, B. A., Bohac, C., Kim, K. H., et al. 2006, *ApJS*, 166, 351
- Chiang, E. I. & Goldreich, P. 1999, *ApJ*, 519, 279
- Churcher, L. J., Wyatt, M. C., Duchêne, G., et al. 2011, *MNRAS*, 417, 1715
- Cieza, L. A., Padgett, D. L., Allen, L. E., et al. 2009, *ApJ*, 696, L84
- D'Alessio, P., Calvet, N., Hartmann, L., Lizano, S., & Cantó, J. 1999, *ApJ*, 527, 893
- David, T. J. & Hillenbrand, L. A. 2015, *ApJ*, 804, 146
- de Grijp, M. H. K., Keel, W. C., Miley, G. K., Goudfrooij, P., & Lub, J. 1992, *A&AS*, 96, 389
- Decin, G., Dominik, C., Malfait, K., Mayor, M., & Waelkens, C. 2000, *A&A*, 357, 533
- Desidera, S. & Barbieri, M. 2007, *A&A*, 462, 345
- Di Francesco, J., Johnstone, D., Kirk, H., MacKenzie, T., & Ledwosinska, E. 2008, *ApJS*, 175, 277
- Dohnanyi, J. S. 1969, *JGR*, 74, 2531
- Dominik, C. & Decin, G. 2003, *ApJ*, 598, 626
- Draine, B. T. & Lee, H. M. 1984, *ApJ*, 285, 89
- Duchêne, G. & Kraus, A. 2013, *ARA&A*, 51, 269
- Duquennoy, A. & Mayor, M. 1991, *A&A*, 248, 485
- Egan, M. P. & Price, S. D. 1996, *AJ*, 112, 2862
- Eiroa, C., Fedele, D., Maldonado, J., et al. 2010, *A&A*, 518, L131
- Eiroa, C., Marshall, J. P., Mora, A., et al. 2013, *A&A*, 555, A11
- Espiau, C., Ingleby, L., Hernández, J., et al. 2012, *ApJ*, 747, 103
- Fitzgerald, M. P., Kalas, P. G., Duchêne, G., Pinte, C., & Graham, J. R. 2007, *ApJ*, 670, 536
- Fixsen, D. J. & Dwek, E. 2002, *ApJ*, 578, 1009
- Gáspár, A., Rieke, G. H., & Balog, Z. 2013, *ApJ*, 768, 25
- Golimowski, D. A., Krist, J. E., Stapelfeldt, K. R., et al. 2011, *AJ*, 142, 30
- Gor'kavyi, N. N., Ozernoy, L. M., Mather, J. C., & Taidakova, T. 1997, *ApJ*, 488, 268
- Greenberg, J. M. 1998, *A&A*, 330, 375
- Habing, H. J., Dominik, C., Jourdain de Muizon, M., et al. 2001, *A&A*, 365, 545
- Harper, D. A., Loewenstein, R. F., & Davidson, J. A. 1984, *ApJ*, 285, 808
- Harris, R. J., Andrews, S. M., Wilner, D. J., & Kraus, A. L. 2012, *ApJ*, 751, 115
- Helou, G. & Walker, D. W. 1988, *Infrared astronomical satellite (IRAS) catalogs and atlases, SSSC*, Vol. 7
- Hillenbrand, L. A., Carpenter, J. M., Kim, J. S., et al. 2008, *ApJ*, 677, 630
- Hindsley, R. B. & Harrington, R. S. 1994, *AJ*, 107, 280
- Holmberg, J., Nordström, B., & Andersen, J. 2009, *A&A*, 501, 941
- Ishihara, D., Onaka, T., Kataza, H., et al. 2010, *A&A*, 514, A1
- Jensen, E. L. N., Mathieu, R. D., & Fuller, G. A. 1996, *ApJ*, 458, 312
- Kalas, P., Graham, J. R., & Clampin, M. 2005, *Natur*, 435, 1067
- Kalas, P., Graham, J. R., Clampin, M. C., & Fitzgerald, M. P. 2006, *ApJ*, 637, L57
- Kelsall, T., Weiland, J. L., Franz, B. A., et al. 1998, *ApJ*, 508, 44
- Kenyon, S. J. & Bromley, B. C. 2001, *AJ*, 121, 538
- \_\_\_\_\_. 2002, *AJ*, 123, 1757
- \_\_\_\_\_. 2004, *AJ*, 127, 513
- Kenyon, S. J. & Hartmann, L. 1987, *ApJ*, 323, 714
- \_\_\_\_\_. 1995, *ApJS*, 101, 117
- Krivov, A. V. 2010, *RAA*, 10, 383
- Li, D., Telesco, C. M., & Wright, C. M. 2012, *ApJ*, 759, 81
- Liu, Q., Wang, T., & Jiang, P. 2014, *AJ*, 148, 3
- Mamajek, E. E. 2012, *ApJ*, 754, L20
- Maness, H. L., Fitzgerald, M. P., Paladini, R., Kalas, P., Duchene, G., & Graham, J. R. 2008, *ApJ*, 686, L25
- Marshall, J. P., Kirchschlager, F., Ertel, S., et al. 2014, *A&A*, 570, A114
- Mason, B. D., Wycoff, G. L., Hartkopf, W. I., Douglass, G. G., & Worley, C. E. 2001, *AJ*, 122, 3466

- Mathieu, R. D., Ghez, A. M., Jensen, E. L. N., & Simon, M. 2000, prpl conf., Protostars and Planets IV, 703
- Metchev, S. A., Eisner, J. A., Hillenbrand, L. A., & Wolf, S. 2005, ApJ, 622, 451
- Mittal, T., Chen, C. H., Jang-Condell, H., Manoj, P., Sargent, B. A., Watson, D. M., & Lisse, C. M. 2015, ApJ, 798, 87
- Mizusawa, T. F., Rebull, L. M., Stauffer, J. R., Bryden, G., Meyer, M., & Song, I. 2012, AJ, 144, 135
- Moór, A., Ábrahám, P., Derekas, A., Kiss, C., Kiss, L. L., Apai, D., Grady, C., & Henning, T. 2006, ApJ, 644, 525
- Moshir, M. & et al. 1990, in IRAS Faint Source Catalogue, version 2.0 (1990), 0
- Najita, J. & Williams, J. P. 2005, ApJ, 635, 625
- Nilsson, R., Liseau, R., Brandeker, A., et al. 2010, A&A, 518, A40
- Panić, O., Holland, W. S., Wyatt, M. C., et al. 2013, MNRAS, 435, 1037
- Pawellek, N., Krivov, A. V., Marshall, J. P., Montesinos, B., Ábrahám, P., Moór, A., Bryden, G., & Eiroa, C. 2014, ApJ, 792, 65
- Pilbratt, G. L., Riedinger, J. R., Passvogel, T., et al. 2010, A&A, 518, L1
- Pollack, J. B., Hollenbach, D., Beckwith, S., Simonelli, D. P., Roush, T., & Fong, W. 1994, ApJ, 421, 615
- Press, W. H., Teukolsky, S. A., Vetterling, W. T., & Flannery, B. P. 1992, in The art of scientific computing(2nd ed. Cambridge, MA: CUP)
- Raghavan, D., Henry, T. J., Mason, B. D., Subasavage, J. P., Jao, W.-C., Beaulieu, T. D., & Hambly, N. C. 2006, ApJ, 646, 523
- Raghavan, D., McAlister, H. A., Henry, T. J., et al. 2010, ApJS, 190, 1
- Reach, W. T., Morris, P., Boulanger, F., & Okumura, K. 2003, Icar164, 384
- Rhee, J. H., Song, I., Zuckerman, B., & McElwain, M. 2007, ApJ, 660, 1556
- Rieke, G. H., Su, K. Y. L., Stansberry, J. A., et al. 2005, ApJ, 620, 1010
- Rieke, G. H., Young, E. T., Engelbracht, C. W., et al. 2004, ApJS, 154, 25
- Roccatagliata, V., Henning, T., Wolf, S., Rodmann, J., Corder, S., Carpenter, J. M., Meyer, M. R., & Dowell, D. 2009, A&A, 497, 409
- Rodriguez, D. R., Duchêne, G., Tom, H., Kennedy, G. M., Matthews, B., Greaves, J., & Butner, H. 2015, MNRAS, 449, 3160
- Rodriguez, D. R. & Zuckerman, B. 2012, ApJ, 745, 147
- Saunders, W., Sutherland, W. J., Maddox, S. J., et al. 2000, MNRAS, 317, 55
- Schneider, G., Silverstone, M. D., & Hines, D. C. 2005, ApJ, 629, L117
- Schneider, G., Silverstone, M. D., Hines, D. C., et al. 2006, ApJ, 650, 414
- Schneider, G., Smith, B. A., Becklin, E. E., et al. 1999, ApJ, 513, L127
- Sheret, I., Dent, W. R. F., & Wyatt, M. C. 2004, MNRAS, 348, 1282
- Smith, R., Churcher, L. J., Wyatt, M. C., Moerchen, M. M., & Telesco, C. M. 2009, A&A, 493, 299
- Song, I., Caillault, J.-P., Barrado y Navascués, D., Stauffer, J. R., & Randich, S. 2000, ApJ, 533, L41
- Steele, A., Hughes, A. M., Carpenter, J., Ricarte, A., Andrews, S. M., Wilner, D. J., & Chiang, E. 2015, ArXiv e-prints
- Su, K. Y. L., Rieke, G. H., Stansberry, J. A., et al. 2006, ApJ, 653, 675
- Thureau, N. D., Greaves, J. S., Matthews, B. C., et al. 2014, MNRAS, 445, 2558
- Tokovinin, A. 2014, AJ, 147, 86
- Trilling, D. E., Bryden, G., Beichman, C. A., et al. 2008, ApJ, 674, 1086
- Trilling, D. E., Stansberry, J. A., Stapelfeldt, K. R., et al. 2007, ApJ, 658, 1289
- Vican, L. 2012, AJ, 143, 135
- Vican, L. & Schneider, A. 2014, ApJ, 780, 154
- Weingartner, J. C. & Draine, B. T. 2001, ApJ, 548, 296
- Weissman, P. R. 1984, Science, 224, 987
- Wolf, S. & Hillenbrand, L. A. 2003, ApJ, 596, 603
- Wyatt, M. C. 2005, A&A, 433, 1007
- Wyatt, M. C., Kennedy, G., Sibthorpe, B., Moro-Martín, A., et al. 2012, MNRAS, 424, 1206
- Yamamura, I., Makiuti, S., Ikeda, N., Fukuda, Y., Oyabu, S., Koga, T., & White, G. J. 2010, VizieR Online Data Catalog, 2298, 0
- Zuckerman, B. & Becklin, E. E. 1993, ApJ, 414, 793